Ion transport in sub-5-nm graphene nanopores

Myung E. Suk[a] and N. R. Aluru[b]
Department of Mechanical Science and Engineering, Beckman Institute for Advanced Science and Technology, University of Illinois at Urbana-Champaign, Urbana, Illinois 61801, USA

(Received 14 November 2013; accepted 10 February 2014; published online 28 February 2014)

Graphene nanopore is a promising device for single molecule sensing, including DNA bases, as its single atom thickness provides high spatial resolution. To attain high sensitivity, the size of the molecule should be comparable to the pore diameter. However, when the pore diameter approaches the size of the molecule, ion properties and dynamics may deviate from the bulk values and continuum analysis may not be accurate. In this paper, we investigate the static and dynamic properties of ions with and without an external voltage drop in sub-5-nm graphene nanopores using molecular dynamics simulations. Ion concentration in graphene nanopores sharply drops from the bulk concentration when the pore radius is smaller than 0.9 nm. Ion mobility in the pore is also smaller than bulk ion mobility due to the layered liquid structure in the pore-axial direction. Our results show that a continuum analysis can be appropriate when the pore radius is larger than 0.9 nm if pore conductivity is properly defined. Since many applications of graphene nanopores, such as DNA and protein sensing, involve ion transport, the results presented here will be useful not only in understanding the behavior of ion transport but also in designing bio-molecular sensors. © *2014 AIP Publishing LLC*. [http://dx.doi.org/10.1063/1.4866643]

I. INTRODUCTION

Ion transport through nanopores has been an emerging area of research. Synthetic nanopores, because of their reduced complexity, serve as a useful model for understanding the permeability and selectivity of biological nanopores.[1,2] High ionic selectivity or permeability of biological nanopores also inspire the development of novel biomimetic synthetic nanopores.[2,3] Ionic current blockades, due to the presence of a single molecule inside a nanopore, have motivated the development of nanopores for single molecule sensing including DNA sequencing.[4]

Graphene nanopore is a promising candidate for DNA sequencing as its thickness is comparable to the distance between base pairs.[5] A nanopore has been drilled in graphene using focused or defocused electron beam irradiation[6] or block copolymer lithography.[7] For high functionality of graphene nanopores, a small pore diameter, comparable to the molecule size, is typically desired. For ion and gas separations, to obtain a high selectivity, the radius of the nanopore should again be comparable to the size of the molecule. For DNA sequencing via ionic current blockade, to attain high sensitivity and lower current noise signal, tightly confining DNA in graphene nanopores of a smaller diameter is preferred. Garaj *et al.*[5] and Schneider *et al.*[8] studied graphene nanopores with diameters ranging from 5 nm to 25 nm. More recently, Garaj *et al.* reported ion transport through a graphene nanopore of 2.5–7 nm in diameter.[9]

When the pore diameter is less than 5 nm, the confined liquid structure in the nanopore affects various transport properties of ions. Such properties may deviate from the bulk properties and continuum analysis based on bulk properties may not be accurate. Ion dynamics and properties are not well understood when they are confined in small pore diameters and atomically thin membranes. In this work, we develop an understanding of the ion dynamics and transport properties using molecular dynamics simulations. Molecular dynamics simulation is a useful tool to observe molecular level details of fluids. Many researchers have studied ion transport through nanopores, focusing on the selectivity, diffusivity, dynamics, etc., using molecular dynamics.[10] In addition, molecular dynamics simulation has been a useful tool for analyzing and interpreting experimental data by tracking the movement of all the molecules in the nanopore over time.[11]

Conductance of ions is an important characteristic property of nanopores. Conductance of ions can be theoretically predicted through a combination of access resistance and pore resistance,[12,13]

$$\frac{1}{G} = R = R_{acc} + R_{pore} = \frac{1}{d\sigma} + \frac{4L}{\pi d^2 \sigma}, \tag{1}$$

where d is the pore diameter, σ is the ion conductivity, and L is the length of the graphene nanopore.

Ion conductivity can be written as

$$\sigma = (\mu_K n_K + \mu_{Cl} n_{Cl}), \tag{2}$$

where μ_K and μ_{Cl} are the mobility of K^+ and Cl^- ions, respectively, and n_K and n_{Cl} are concentration of K^+ and Cl^- ions, respectively.

In analysis of nanopore conductance, theoretical models have been used with bulk conductivity.[5,13] Garaj *et al.*

[a]Present address: Korea Railroad Research Institute, Uiwang-si, Gyeonggi-do, South Korea.
[b]Author to whom correspondence should be addressed. Electronic mail: aluru@illinois.edu. URL: http://www.illinois.edu/~aluru/.

fitted experimental conductance data of a graphene nanopore to a theoretical model (Laplace equation) by using the bulk conductivity and adjusting the membrane length and pore diameter.[5,9] However, when the pore diameter is reduced to a size comparable to the size of an ion, bulk conductivity may not be valid and this may result in an inaccurate measurement of the pore dimensions.

Due to the lower conductance found in graphene nanopores compared to the theoretical model for a small pore radius, the possibility of reduced conductivity is noted in Ref. 14. However, the source of the discrepancy was not well understood. The existence of concentration polarization or limited reservoir dimension used in the simulation is conjectured as the source of the discrepancy.[14] Thus, understanding the validity of the theoretical model and graphene nanopore conductivity will be essential for graphene nanopores of smaller diameters.

In this study, we found that the theoretical model is valid for nanopores with a pore radius larger than ~0.9 nm if the local ionic conductivity in graphene nanopores is properly assessed. The source of discrepancy between ionic conductivity in graphene nanopores and the bulk ionic conductivity was found to be due to the ion partitioning arising from steric hindrance and low ionic mobility, possibly due to the layered liquid structure in the pore axial direction. The discrepancy is negligible if the pore radius is larger than ~9 nm and the theoretical continuum model captures the reported nanopore conductance reasonably well. Additionally, the contribution of pore resistance and access resistance was identified to resolve the controversial dependency of conductance on pore radius.

II. METHODS

We performed equilibrium molecular dynamics (EMD) simulations to investigate ion concentration and mobility in graphene nanopores. We also performed non-equilibrium molecular dynamics (NEMD) simulations by applying an external voltage drop to investigate ion currents and conductance of graphene nanopores. Figure 1 shows a simulation setup. A graphene nanopore is located at the center of the simulation box, which is filled with water and 1 M KCl. The pore radii that we considered in this work are 0.283 nm, 0.424 nm, 0.704 nm, 0.933 nm, 1.169 nm, 1.511 nm, 1.888 nm, and 2.462 nm. Pore radius was determined by measuring the distance from the pore axis to the location where the liquid density dropped to below 2% of the bulk value. In this way, the accessible pore area for water and ions is well-represented.[15] The corresponding center-to-center radii calculated by averaging the distance from the pore axis to the center of the carbon atoms in the pore edge are 0.424 nm, 0.526 nm, 0.911 nm, 1.136 nm, 1.374 nm, 1.687 nm, 2.083 nm, and 2.628 nm.

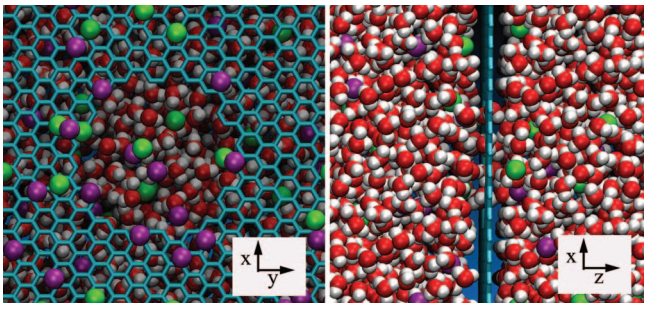

FIG. 1. Snapshot of a MD simulation of ion transport through a graphene nanopore. Graphene membrane is shown in blue. Water molecules are represented by red (oxygen) and white (hydrogen) spheres. K^+ and Cl^- ions are represented by purple and green spheres, respectively. Overhead view of simulation box (left). Water molecules in the top reservoir are removed to show the nanopore. Nanopore radius is $R = 0.704$ nm. Side view of the simulation box (right).

Both the x and y dimensions of the graphene membrane range from about 4 nm to 10 nm in length depending on the pore radius in order to maintain constant porosity (pore area/total membrane area). The z dimension of the total system is approximately 6–10 nm in length. Graphene pores are generated by removing atoms whose coordinates satisfy the condition $(x - C_x)^2 + (y - C_y)^2 < R^2$, where C_x and C_y are the x and y coordinates of the pore center, respectively. The carbon atoms of the graphene membrane are modeled as Lennard-Jones (LJ) spheres with the parameters $\sigma_{C\text{-}C} = 0.339$ nm and $\varepsilon_{C\text{-}C} = 0.0692$ kcal/mol.[16] Water molecules are modeled using the simple point charge-extended (SPC/E) water model.[17] Polarization of water molecules was found to be negligible with field strength less than 10 V/nm.[18] LJ parameters for ions are taken from Joung and Cheatham, where a water-specific force field was developed.[19] With SPC/E water, LJ parameters for K are $\sigma_{K\text{-}K} = 0.284$ nm and $\varepsilon_{K\text{-}K} = 0.430$ kcal/mol. For Cl, $\sigma_{Cl\text{-}Cl} = 0.483$ nm and $\varepsilon_{Cl\text{-}Cl} = 0.0128$ kcal/mol. Lorentz-Berthelot mixing rules are used for interaction between different species. The total number of water molecules varied from 2968 to 30 871 and the number of ions varied from 120 to 1200 depending on the size of the system.

Simulations were performed using the LAMMPS package. An *NVT* ensemble was used with periodic boundary condition in all the three-directions. The Velocity-Verlet algorithm was used for integration with a time step of 2 fs. A Nosé-Hoover thermostat was used to maintain the temperature at 300 K with a time constant of 0.1 ps. Graphene membranes were kept rigid during the simulation by fixing carbon atoms to their lattice positions. We tested the flexible graphene membrane by applying the AIREBO potential. It did not significantly affect the simulation results for molecular permeation and transport through the graphene nanopore. The carbon atoms stay in their lattice sites with negligible displacement due to the strong sp^2 bonds. Particle-particle particle-mesh (PPPM) method was used for long range electrostatics. A shake algorithm was used to constrain the angle and bond length of SPC/E water. Initially, all simulations were run for 500 ps for equilibration. Three separate equilibration configurations were run for a total of 15-30 ns for data production in EMD. NEMD simulations were run for a total of 15 ns by applying an external voltage drop ranging from 1.5 V to 6 V. The mean values are calculated by averaging six subtrajectories. The error bar was estimated from the standard error.

III. RESULTS AND DISCUSSION

A. Ion hydration in graphene nanopores

First, we investigated ion hydration in graphene nanopores. Due to the strong electrostatic interaction between ions and polar water molecules, an ion hydration shell is observed. We measured the hydration radius by investigating the radial density distribution of water molecules around ions as shown in Figure 2. The first density peak in the radial distribution indicates the first hydration shell. The first minimum after the first density peak is measured as the ion hydration radius. The first hydration radius of K^+ and Cl^- in bulk water is 0.36 nm and 0.38 nm, respectively, which is in good agreement with the reported values (0.362 nm and 0.385 nm for K^+ and Cl^-, respectively[20]).

The ion hydration number was also examined by counting the water molecules in the first hydration shell. Approximately seven water molecules occupied the first hydration shell for both ions in bulk liquids. The ion hydration number was reduced when the pore radius was smaller than 0.9 nm (see Figure 3 inset). However, the reduction is small, i.e., a coordination number of 6.6 is observed for the smallest nanopore radius considered (R_p = 0.3 nm). Most of the hydration shells of the ions are conserved by leaving them outside the pore and, hence, the reduction of the coordination number is small. The hydration number reduction was much larger in thicker nanoporous membranes with the same radius. For example, the hydration number is reduced by one water molecule when ions were confined in the carbon nanotube with a similar radius.[21]

B. Partition coefficient of graphene nanopores

As the pore diameter gets smaller and approaches the hydration diameter or bare ionic diameter, ion concentration in the graphene nanopore is significantly reduced from the bulk concentration due to the free energy barrier. The ion partition

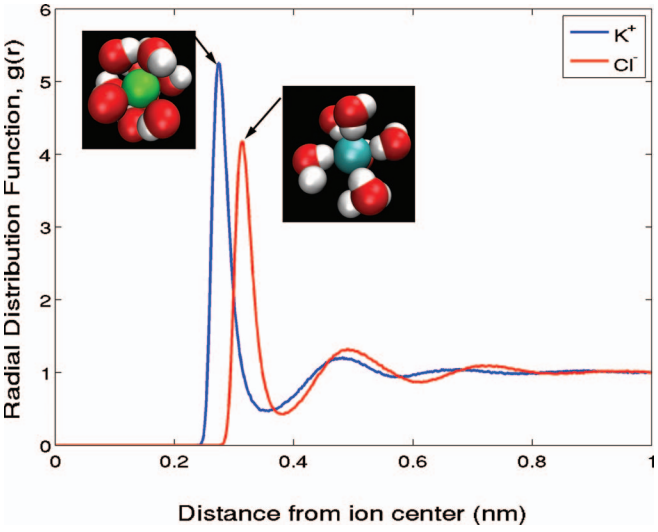

FIG. 2. The radial distribution function of water molecules around K^+ and Cl^-. The first minimum from the center is taken to be the ion hydration radius. The snapshots show the ion hydration shell around K^+ and Cl^-.

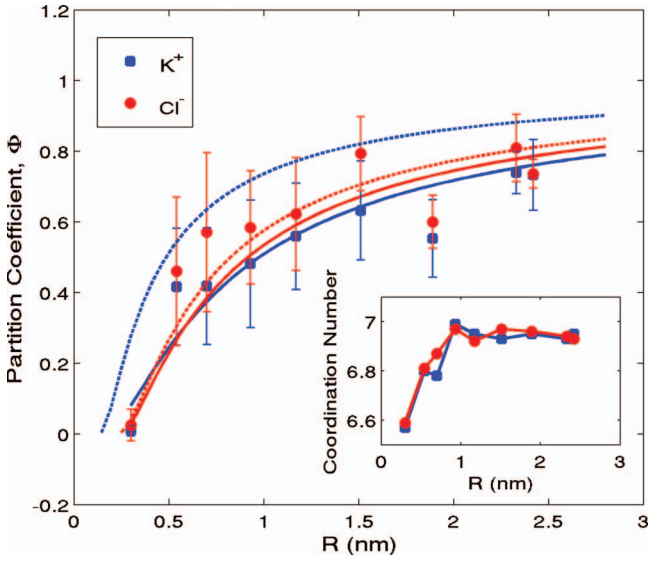

FIG. 3. Partition coefficient of K^+ and Cl^- with pore radius. Dashed lines indicate the partition coefficient as a result of the steric hindrance only. Solid lines indicate the partition coefficient as a result of the steric hindrance and hydration free energy loss (Eq. (4)). Inset: Ion coordination number for K^+ and Cl^-.

coefficient can be determined by

$$\Phi = \frac{c_p}{c_b}, \tag{3}$$

where c_p is the pore concentration and c_b is the bulk concentration. Ion concentration can be calculated by $c = N/V$, where N is the number of ions in the cylindrical bin defining the pore (the radius and length of the cylindrical bin are the pore radius and length, respectively) and V is the bin volume. Partition coefficients obtained from the equilibrium MD simulation are plotted in Figure 3. As the pore radius increases, the partition coefficient increases and approaches unity indicating that the pore concentration approaches the bulk concentration.

Since the pore surface is not charged, the main mechanism of ion partitioning is steric exclusion and dehydration effect, expressed as

$$\Phi = (1-\lambda)^2 \exp\left(\frac{\Delta G_h}{k_B T}\right), \tag{4}$$

where Φ is the ion partition coefficient, λ is the ratio of the solute radius to the pore radius, and ΔG_h is the molecular free energy of dehydration. The first term, $(1-\lambda)^2$, computes ion partitioning due to steric exclusion and its contribution is plotted with dashed lines in Figure 3. The free energy of dehydration is often calculated together with Born energy, the electrical potential energy of charged spheres in the dielectric medium. From the continuum dielectric model, free energy loss scales as $1/R$.[22] By fitting the partition coefficient obtained from the equilibrium MD simulation to Eq. (4), ΔG_h is determined as $0.37/R$ k_BT/nm and $0.075/R$ k_BT/nm for K^+ and Cl^-, respectively, which are very small compared to the total free energy of dehydration (80 k_BT and 90 k_BT for K^+ and Cl^-, respectively) or the steric exclusion term.

In contrast to a conventional nanofiltration membrane, where dielectric exclusion is a dominant factor,[23] steric exclusion was found to be a dominant factor in ion partitioning, probably due to the atomically thin membrane length whose effect on ion hydration environment (or dielectric environment) is small. However, steric hindrance alone cannot explain the higher concentration of larger Cl^- over the smaller K^+ in the graphene nanopore. We found that the dehydration-free energy penalty was almost negligible for the larger Cl^-. Due to the weaker electrostatic interaction between ions and water molecules, larger ions tended to adjust to the hydration shell with a lower free energy cost than smaller ions. As a result, ion partitioning is higher for larger Cl^- than for smaller K^+.

C. Ion mobility in graphene nanopore

The diffusion coefficient of ions in a graphene nanopore is calculated and plotted in Figure 4(a). We found that the diffusion coefficient of ions confined in a graphene nanopore scales as $(1/D_p - 1/D_{bulk}) \sim 1/R_p$, where D_p and D_{bulk} are the diffusion coefficients of ions in a nanopore and in bulk liquid, respectively, and R_p is the pore radius. The bulk ion diffusion coefficients were also calculated and they are 1.71×10^{-9} m^2/s and 1.62×10^{-9} m^2/s for K^+ and Cl^-, respectively, which are in reasonable agreement with the reported diffusivity[20] (1.89×10^{-9} m^2/s for K^+ and 1.66×10^{-9} m^2/s for Cl^-). Ion mobility was calculated from diffusivity and is plotted in Figure 4(b). Variation in ion mobility with pore radius can be expressed as

$$\mu_{pore} = \left(\frac{C}{R} + \frac{1}{\mu_{bulk}}\right)^{-1}, \tag{5}$$

C is determined as 4.104×10^{-3} V · s/m and 6.215×10^{-3} V · s/m for K^+ and Cl^-, respectively, using least-squares fitting. The decreased mobility in graphene nanopores is related to the liquid structure near the graphene nanopores. A decreased diffusion coefficient of water molecules in a graphene nanopore was observed to be due to the layered water structure in the pore axial direction.[15,24] Similarly, ion mobility also decreases from the bulk value due to the layered liquid structure in the pore axial direction. When the pore diameter was about 0.5 nm, mobility is reduced from the bulk value by about 40%. The reduced ion mobility in the graphene nanopore is in contrast to a 100-times higher ion mobility, compared to the bulk ion mobility, in a carbon nanotube.[25] As expected, the layered liquid structure in the axial direction was not found in the interior of long carbon nanotubes.

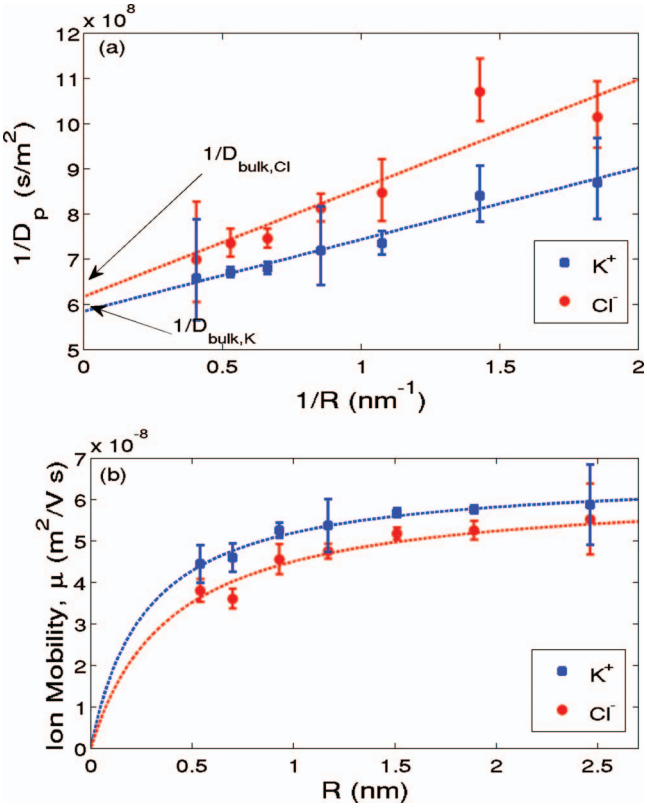

FIG. 4. (a) The reciprocal of the diffusion coefficient of ions varies linearly with the reciprocal of the pore radius. (b) Ion mobility with pore radius. Mobility increases monotonically and approaches the bulk mobility as the pore radius increases.

D. Conductance of graphene nanopores

A NEMD with an external voltage drop was performed to measure the ionic conductance. The ionic current was determined by counting the number of ions translocating across the membrane. The ionic current (I) as a function of the applied voltage drop (V) is shown in Figure 5(a). The I–V curve is linear up to a voltage drop of 3 V and conductance is determined from the linear slope. The conductance obtained from NEMD simulations as a function of the pore radius is shown in Figure 5(b). In sub-5-nm graphene nanopores, conductance reaches 41.2 nS. In the smallest nanopore of $R_p = 0.3$ nm, the conductance is ~0.6 nS.

The conductance obtained from NEMD is also compared to the theoretical model (Eq. (1)) by inserting the bulk conductivity and the pore conductivity. The variation of the pore conductivity with pore radius is calculated with the ion density and mobility partition coefficient as

$$\sigma_{pore}(R) = \Phi(R)\Gamma(R)\sigma_{bulk}, \tag{6}$$

where $\Phi(R)$ is the density partition coefficient (Eq. (4)) and $\Gamma(R)$is the mobility partition coefficient defined as μ_{pore}/μ_{bulk} (Eq. (5)). Pore length (membrane thickness) is defined to be 0.535 nm from the water density profile (see Ref. 15 for details on the definition of the length of the pore). To be consistent with the definition of pore radius, the membrane surface is defined as the location where the water molecule density dropped below 2% of bulk density. This is somewhat larger than the carbon diameter of 0.34 nm. As shown in Figure 5(b), the ionic conductance is described well by the continuum theory if the pore size dependent conductivity is considered. However, with the bulk conductivity, the continuum theory fails to predict the ionic current in graphene nanopores.

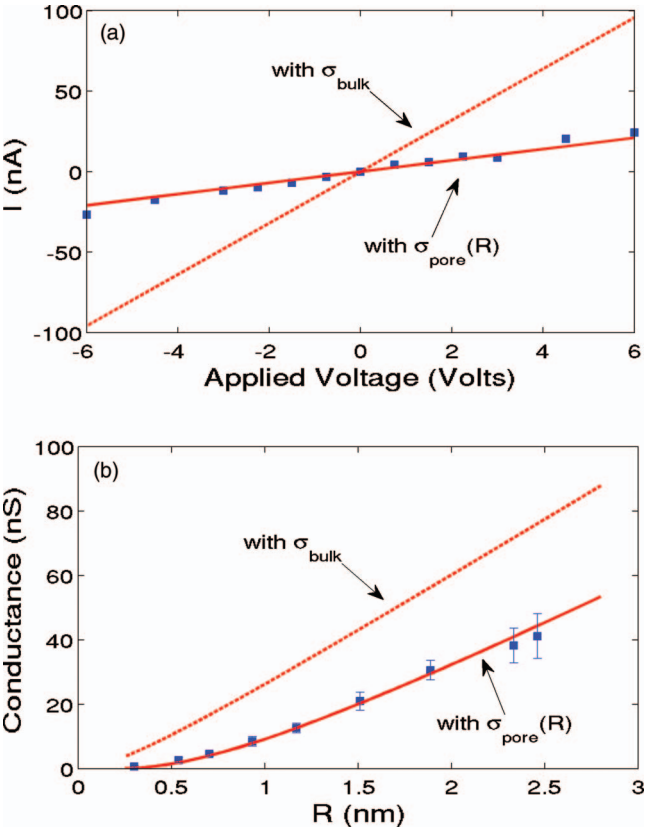

FIG. 5. (a) *I-V* curve for a graphene nanopore. Pore radius is 0.7 nm. Current increases linearly with voltage up to 3 V. (b) Ionic conductance obtained from the slope of the *I-V* curve in the linear region. The dashed line is the continuum model with bulk conductivity and the solid lines are the continuum model with pore conductivity calculated from Eq. (6).

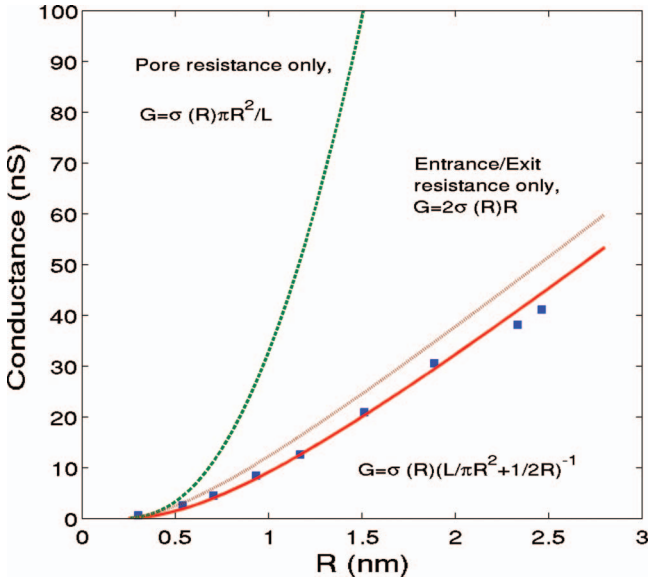

FIG. 6. The contribution of pore resistance and entrance/exit resistance. Green line is conductance with pore resistance only. Blue line is conductance with entrance/exit resistance only. Red line is conductance with both pore resistance and entrance/exit resistance. Blue squares are MD data. In the case of graphene nanopores, entrance/exit resistance is more dominant. However, due to the varying pore conductivity, conductance shows mild nonlinear behavior.

We also examined the contribution of entrance/exit (access) resistance and pore resistance. According to Eq. (1), if the pore aspect ratio (pore diameter/pore length) is large, access resistance is dominant and conductance linearly depends on the pore radius. On the other hand, if the pore aspect ratio is small, access resistance is negligible and conductance depends quadratically on the pore radius. This scaling has been controversial, as Garaj *et al.* have argued that the conductance of graphene nanopores follows linear scaling,[5] while Sathe *et al.* and Schneider *et al.* used quadratic scaling to fit their data.[8] This controversy might be due to the variation in pore conductivity. The contribution of pore resistance and entrance/exit resistance is separately plotted in Figure 6 with simulation results. The green line indicates the conductance with the pore resistance only and the blue line indicates the conductance with entrance/exit resistance only. Red line indicates the conductance by considering both the entrance/exit and the pore resistance, which is in good agreement with MD data shown by the blue squares. As shown in the figure, entrance/exit resistance is dominant in graphene nanopores and conductance shows near linear behavior. However, it does not follow a perfect linear scaling due to the variation of pore conductivity rather than the contribution of pore resistance. In fact, conductance calculated when considering only the entrance/exit resistance deviates from linearity as the pore radius decreases.

E. Subcontinuum to semicontinuum to continuum transition

We modified the continuum theory with pore radius dependent conductivity, which is referred to as a semicontinuum model. We further compared the continuum and semicontinuum models with the data in literature in Figure 7. In Figure 7, the continuum model and the semicontinuum model are represented by dashed lines and solid lines, respectively. Open pore conductance of 1M KCl was experimentally measured by Garaj *et al.*[5] (blue triangles) and Schneider *et al.*[8] (blue circles). It was also determined by Sathe *et al.* (blue squares) using MD simulation.[26] Conductance data obtained in this study are also shown in Figure 7 (blue diamonds). The semicontinuum model provides very good agreement with the MD results reported by Sathe *et al.* Experimental data by Schneider *et al.* are lower than both the continuum and semicontinuum models. This discrepancy may be attributed to the measurement errors of the pore radius or surface condition. The experimental data from Garaj *et al.* provide a reasonable agreement with the theoretical model as their data falls between the continuum and semicontinuum models. The pore diameter considered by Garaj *et al.* is larger than 5 nm. In that case, the difference between the continuum and semicontinuum models is less than 20% and experimentally not very significant compared to experimental error/variance. Garaj *et al.* reported pore conductance with a larger concentration (3M) and for smaller pore diameters of (2–7 nm) in a recent paper.[9] They are represented by red circles and squares in Figure 7. The results from the continuum model (red dashed line) and the semicontinuum mode (red solid line) are also shown. For this range of pore diameters, the experimental data are closer to

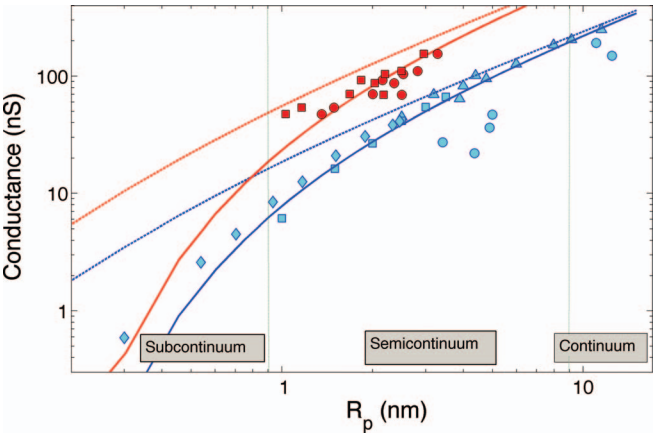

FIG. 7. A comparison of the theoretical model for conductance from the present and previous studies.[5,8,9,26] Dashed lines indicate the continuum model with bulk ion conductivity. Solid lines indicate the semicontinuum model with conductivity dependent on the pore radius. Blue data points and lines are for 1 M KCl. Red data points and lines are for 3 M KCl. Red squares are with pore radius measured with TEM image. Red circles represent effective pore radius obtained by subtracting 0.325 nm from the radius measured with TEM image.[9] When pore radius is above ∼9 nm, the continuum model reasonably agrees with the conductance data. For pore radius smaller than ∼9 nm, continuum model deviates from the conductance data and the semicontinuum model agrees with the conductance data (shown as semicontinuum region in the plot). For pore radius smaller than ∼0.9 nm, the conductance data deviates from the semicontinuum model (deviation of more than 10% is observed). In this case the subcontinuum model is necessary.

the semicontinuum model and the results from the continuum model deviate by ∼60% from the experimental data.

The semicontinuum model deviates from the conductance data as the pore radius decreases and approaches the molecular scale. The difference between conductance data and the semicontinuum model is larger than 10% when the pore radius is smaller than 0.9 nm. When the pore radius is smaller than ∼0.9 nm, this is defined as the subcontinuum regime. In this regime, the subcontinuum approach, such as the rate theory, provides a better approximation of pore conductance. As with the water permeation rate, ionic conductance can be obtained by calculating the equilibrium rate coefficients of ions as follows:[27]

$$G = (k_{0,\mathrm{K}} + k_{0,\mathrm{Cl}})\frac{q^2}{k_B T}, \tag{7}$$

where k_0 are equilibrium rate coefficients. The conductance computed by the rate theory is 0.69 nS and 3.1 nS for 0.3 nm and 0.54 nm radii pores, respectively. They are much closer to the conductance values of 0.59 nS and 2.6 nS obtained from nonequilibrium MD simulation. In contrast, the conductance values obtained from the semicontinuum models are 0.17 nS and 1.8 nS, respectively.

For a sufficiently large pore radius, the continuum approach based on bulk conductivity can be accurate. The error from the continuum model can be calculated as $\%\mathrm{error} = 1 - \Phi(R_P)\Gamma(R_P)$. If the error criterion is 10%, the semicontinuum-to-continuum transition occurs at a pore radius of around 9 nm. If the error criterion is 5%, the semicontinuum-to-continuum transition occurs at a pore radius of around 17 nm. In experimental studies on graphene nanopores, mostly nanopores in the continuum regime were examined. However, as a smaller pore radius is more desirable for DNA sequencing applications or molecular sieving applications, semicontinuum and subcontinuum approaches may be necessary in order to predict and properly design graphene nanopores.

In this study, we only tested bare (non-functionalized) graphene nanopore to develop a fundamental understanding of ion transport through an atomically thin graphene membrane. However, ion transport through functionalized graphene nanopores is also a topic of great interest. The altered chemistry at the pore edge by means of functionalization would affect ion transport through the graphene nanopore. For example, Sint and co-workers[28] studied graphene nanopore functionalized with negatively charged nitrogens and fluorines, which showed cation selectivity. They also studied positively charged hydrogens, which showed anion selectivity. Konatham and co-workers[29] studied functionalized pores with COO^-, $NH3^+$, and OH groups and investigated the effect of functional group on ion rejection. He and co-workers[30] examined graphene nanopore functionalized with COO^- group to achieve selectivity of K^+ ions over Na^+ ions. As a future study, our work can be expanded for theoretical understanding and modeling of functionalized graphene nanopores.

IV. CONCLUSIONS

In this study, monovalent ion transport and dynamics in graphene nanopores was studied with and without the application of an external voltage drop. In equilibrium condition, ion concentration in graphene nanopores drops sharply from the bulk concentration when the pore radius is smaller than 0.9 nm. The main contribution to ion partitioning was found to be steric exclusion. The contribution of dielectric exclusion to ion partitioning was small, but it resulted in a slightly higher concentration for the larger Cl^- ions than for the K^+ ions. Ion mobility is smaller than bulk ion mobility due to the layered liquid structure in the pore-axial direction. By modifying the ionic conductivity with the local density and mobility partition coefficient, the continuum description predicts the ionic conductance reasonably well for pore radius larger than 0.9 nm. For pore radius smaller than 0.9 nm, rate theory provides a better estimation of ionic conductance, indicating the transition to a subcontinuum regime. The discrepancy in pore and bulk conductivity is negligible when the pore radius is larger than 9 nm, indicating a continuum regime. Since many applications of graphene nanopores, such as DNA sensing and protein sensing, involve ion transport driven by electric field, the results presented here will be useful not only in understanding the ion transport behavior but also in predicting and designing bio-molecular sensors.

ACKNOWLEDGMENTS

This work is supported by the (U.S.) Air Force Office of Scientific Research (USAFOSR) and the National Science Foundation (NSF) under Grant No. 1264282. The authors gratefully acknowledge the use of the parallel computing resource provided by the University of Illinois. This work used the Extreme Science and Engineering Discovery Environment

(XSEDE), which is supported by the National Science Foundation Grant No. OCI-1053575.

[1]F. Zhu and K. Schulten, Biophys. J. **85**, 236 (2003).
[2]S. W. Kowalczyk, T. R. Blosser, and C. Dekker, Trends Biotechnol. **29**, 607 (2011).
[3]E. C. Yusko, J. M. Johnson, S. Majd, P. Prangkio, R. C. Rollings, J. Li, J. Yang, and M. Mayer, Nat. Nanotechnol. **6**, 253 (2011).
[4]B. M. Venkatesan and R. Bashir, Nat. Nanotechnol. **6**(10), 615 (2011).
[5]S. Garaj, W. Hubbard, A. Reina, J. Kong, D. Branton, and J. A. Golovchenko, Nature (London) **467**(7312), 190 (2010).
[6]B. Song, G. F. Schneider, X. Qiang, P. Gregory, C. Dekker, and Z. Henny, Nano Lett. **11**(6), 2247 (2011); C. J. Russo and J. A. Golovchenko, Proc. Natl. Acad. Sci. U.S.A. **109**(16), 5953 (2012).
[7]M. Kim, N. S. Safron, E. Han, M. S. Arnold, and P. Gopalan, Nano Lett. **10**(4), 1125 (2010).
[8]G. F. Schneider, S. W. Kowalczyk, V. E. Calado, G. Pandraud, H. W. Zandbergen, L. M. K. Vandersypen, and C. Dekker, Nano Lett. **10**(8), 3163 (2010).
[9]S. Garaj, S. Liu, D. Branton, and J. A. Golovchenko, in e-print arXiv:1204.4361v2 (2012); S. Garaj, S. Liu, J. Golovchenko, and D. Branton, Proc. Natl. Acad. Sci. U.S.A. **110**, 12192 (2013).
[10]O. Beckstein, K. Tai, and M. S. P. Sansom, J. Am. Chem. Soc. **126**(45), 14694 (2004); S. Joseph, R. J. Mashl, E. Jakobsson, and N. R. Aluru, Nano Lett. **3**(10), 1399 (2003).
[11]X. Peng, J. Jin, Y. Nakamura, T. Ohno, and I. Ichinose, Nat. Nanotechnol. **4**(6), 353 (2009).
[12]J. E. Hall, J. Gen. Physiol. **66**, 531 (1975).
[13]S. W. Kowalczyk, A. Y. Grosberg, Y. Rabin, and C. Dekker, Nanotechnology **22**, 315101 (2011).
[14]G. Hu, M. Mao, and S. Ghosal, Nanotechnology **23**, 395501 (2012).
[15]M. E. Suk and N. R. Aluru, RSC Adv. **3**, 9365 (2013).
[16]G. Chen, Y. Guo, N. Karasawa, and W. A. Goddard, III, Phys. Rev. B **48**(18), 13959 (1993).
[17]H. J. C. Berendsen, J. R. Grigera, and T. P. Straatsma, J. Phys. Chem. **91**(24), 6269 (1987).
[18]K. Yang, S. Yiacoumi, and C. Tsouris, J. Chem. Phys. **117**, 337 (2002).
[19]I. S. Joung and T. E. Cheatham, J. Phys. Chem. B **112**, 9020 (2008).
[20]I. S. Joung and T. E. Cheatham, J. Phys. Chem. B **113**, 13279 (2009).
[21]C. Song and B. Corry, J. Phys. Chem. B **113**, 7642 (2009).
[22]A. Parsegian, Nature **221**, 844 (1969).
[23]C. Tu, Y. Fang, Z. Zhu, B. Van der Bruggen, and X. Wang, Langmuir **27**, 10274 (2011).
[24]M. E. Suk and N. R. Aluru, J. Phys. Chem. Lett. **1**(10), 1590 (2010).
[25]C. Y. Lee, W. Choi, J.-H. Han, and M. S. Strano, Science **329**(5997), 1320 (2010).
[26]C. Sathe, X. Zou, J. P. Leburton, and K. Schulten, ACS Nano **5**(11), 8842 (2011).
[27]B. L. De Groot and H. Grubmuller, Curr. Opin. Struct. Biol. **15**, 176 (2005).
[28]K. Sint, B. Wang, and P. Král, J. Am. Chem. Soc. **130**(49), 16448 (2008).
[29]D. Konatham, J. Yu, T. A. Ho, and A. Striolo, Langmuir **29**(38), 11884 (2013).
[30]Z. He, J. Zhou, X. Lu, and B. Corry, ACS Nano **7**(11), 10148 (2013).